27. Lin, W. C., Chen, A. C., Tseng, C. J. and Hwang, S. G., An investigation and study of Chinese tallow tree in Taiwan (*Sapium sebiferum* Roxb.). *Bull. Taiwan For. Res. Inst.*, 1958, **67**, 1–37.
28. Cameron, G. N. and Spencer, S. R., Rapid leaf decay and nutrient release in a Chinese tallow forest. *Oecologia*, 1989, **80**(2), 222–228.
29. Hosking, J. R., Conn, B. J. and Lepschi, B. J., Plant species first recognised as naturalised for New South Wales over the period 2000–2001. *Cunninghamia*, 2003, **8**, 175–187.
30. Jaryan, V., Chopra, S., Uniyal, S. K. and Singh, R. D., Spreading fast yet unnoticed: are we in for another invasion? *Curr. Sci.*, 2007, **93**, 1483–1484.
31. Rao, R. R., *Biodiversity in India* (*Floristic Aspects*). Bishen Singh Mahendra Pal Singh, Dehradun (reprinted), 2006.
32. Jaryan, V., Uniyal, S. K., Kumar, A., Gupta, R. C., Parkash, O. and Singh, R. D., Distribution characteristics of *Sapium sebiferum* (L.) Roxb. – an invasive tree species in Himachal Pradesh, western Himalaya. *Proc. Indian Natl. Sci. Acad*, 2013, **79**(2), 215–234.
33. Pattison, R. R. and Mack, R. N., Potential distribution of the invasive tree *Triadica sebifera* (Euphorbiaceae) in the United States: evaluating CLIMEX predictions with field trials. *Global Change Biol.*, 2008, **14**, 813–826.
34. Jaryan, V., Uniyal, S. K., Gupta, R. C. and Singh, R. D., Extent of occurrence and area of occupancy of tallow tree (*Sapium sebiferum*): using the red list criteria for documenting invasive species expanse. *Natl. Acad. Sci. Lett*., 2013, **36**, 85–91.
35. Peterson, A. T., Papes, M. and Kluza, D. A., Predicting the potential invasive distributions of four alien plant species in North America. *Weed Sci*., 2003, **51**, 863–868.
36. Stohlgren, T. J., Ensemble habitat mapping of invasive plant species. *Risk Anal*., 2010, **30**(2), 224–235.
37. Scheldeman, X. and Zonneveld, Mv., *Training Manual on Spatial Analysis of Plant Diversity and Distribution*, Biodiversity International, Rome, 2010.
38. Dormann, C. F. *et al.*, Methods to account for spatial autocorrelation in the analysis of species distributional data: a review. *Ecographysics*, 2007, **30**, 609–628.
39. Kumar, P., Assessment of impact of climate change on rhododendrons in Sikkim Himalaya using Maxent modeling: limitations and challenges. *Biodivers. Conserv.*, 2012, **21**, 1251–1266.
40. ESRI, ArcGIS 8.3, User Manuals, Redlands, USA, 2002.
41. Fielding, A. H. and Bell, J. F., A review of methods for assessment of prediction errors in conservation presence/absence models. *Environ. Conserv.*, 2007, **24**, 38–49.
42. Khanum, R., Mumtaz, A. S., and Kumar, S., Predicting impacts of climate change on medicinal asclepiads of Pakistan using Maxent modeling. *Acta Oecol.*, 2013, **49**, 23–31.
43. Anderson, R. P., Lew, D. and Peterson, A. T., Evaluating predictive models of species' distributions: criteria for selecting optimal models. *Ecol. Model.*, 2003, **162**, 211–232.
44. Swets, J. A., Measuring the accuracy of diagnostic systems. *Science*, 1988, **240**, 1285–1293.
45. Peterson, A. T., Predicting the geography of species invasions via ecological niche modeling. *Q. Rev. Biol.*, 2003, **78**(4), 419–433.
46. Jimenez-Valverde, A. J., Peterson, A. T., Soberon, J., Overton, J. M., Aragon, P. and Lobo, J. M., Use of niche models in invasive species risk assessments. *Biol. Invas*., 2011, **13**, 2785–2797.
47. Jubinsky, G., Chinese tallow gets worse! *Palmetto*, 1993, **13**, 3.
48. Murty, S. K., *Flora of Cold Deserts of Western Himalaya*. *Volume 1* (*Monocotyledons*), Botanical Survey of India, Calcutta, 2001, pp. 452.
49. Khan, M., Kumar, S. and Hamal, I. A., Medicinal plants of Sewa river catchment area in the North west Himalaya and its implication for conservation. *Ethnobot. Leaflets*, 2009 **13**, 1113–1139.
50. Negi, P. S. and Hajra, P. K., Alien flora of Doon Valley, Northwest Himalaya. *Curr. Sci.*, 2007, **92**(7), 968–978.
51. Barrilleaux, T. C. and Grace, J. B., Growth and invasive potential of *Sapium sebiferum* (Euphorbiaceae) within the coastal Prairie region: the effect of soil and moisture regime. *Am. J. Bot*., 2000, **87**(8), 1099–1106.
52. Hsu, B. H., A systematic examination of Chinese tallow seeds and oil. *China J*., 1928, **9**, 244–251.
53. Burns, J. H. and Miller, T. E., Invasion of Chinese tallow (*Sapium sebiferum*) in the Lake Jackson area, northern Florida. *Am. Midl. Nat*., 2004, **152**(2), 410–417.
54. Bruce, K. A., Cameron, G. N. and Harcombe, P. A., Initiation of a new woodland type on the Texas coastal prairie by the Chinese tallow tree (*Sapium sebiferum* (L.) Roxb). *Bull. Torrey Bot. Club*, 1995, **122**, 215–225.

ACKNOWLEDGEMENTS. We thank the Director CSIR-IHBT, Palampur for providing facilities and encouragement, and the staff and faculty of CSIR-IHBT herbarium for fruitful discussions. V.J. thanks the Council of Scientific and Industrial Research, New Delhi for Senior Research Fellowship. We acknowledge the constructive comments of the editor and the two anonymous reviewers that helped improve the manuscript. This is IHBT communication number 3410.

Received 26 March 2013; revised accepted 28 August 2013

Crevasses detection in Himalayan glaciers using ground-penetrating radar

K. K. Singh[1,*], H. S. Negi[1], A. Ganju[1], A. V. Kulkarni[2], A. Kumar[3], V. D. Mishra[1] and S. Kumar[1]

[1]Snow and Avalanche Study Establishment, Chandigarh 160 036, India
[2]Divecha Centre for Climate Change, Indian Institute of Science, Bangalore 560 012, India
[3]National Institute of Technology, Kurukshetra 136 119, India

Identification and mapping of crevasses in glaciated regions is important for safe movement. However, the remote and rugged glacial terrain in the Himalaya poses greater challenges for field data collection. In the present study crevasse signatures were collected from Siachen and Samudra Tapu glaciers in the Indian Himalaya using ground-penetrating radar (GPR). The surveys were conducted using the antennas of 250 MHz frequency in ground mode and 350 MHz in airborne mode. The identified signatures of open and hidden crevasses in GPR profiles collected in ground mode were validated by ground truthing. The crevasse zones and buried boulder areas in a glacier were identified using a combination of airborne GPR profiles and SAR data, and the same have been validated with the high-resolution optical satellite imagery (Cartosat-1) and Survey of India mapsheet. Using multi-sensor data, a crevasse map for Samudra Tapu glacier was prepared. The present methodology can also be used for mapping the crevasse zones in other glaciers in the Himalaya.

*For correspondence. (e-mail: kamal.kant@sase.drdo.in)

Keywords: Crevasses detection, glaciers, ground-penetrating radar.

A CREVASSE is usually perceived as a large crack in the ice, which may either be open or hidden by snow. Crevasses of different dimensions are formed by tensional stress acting upon the brittle ice[1]. Crevasses are mostly formed when the glacier mass at its middle and sides move at different rates or curves around a bend. The abrupt change in terrain slope and increase in the rate of movement of glacier ice are factors responsible for crevasse formation. They can be deep and dangerous for human activity in glaciated areas, especially when they are buried under snow and are not visible. The orientation of crevasses can be correlated with the surface strain rate and thus can be used to understand the ice dynamics[2–5].

The crevasses buried by the accumulation of seasonal snow are called the hidden crevasses. Detection of hidden crevasses in glaciers is important, as they are not visible and a person might easily get trapped in it while moving through the region. These buried crevasses were detected using radio echo sounding techniques, i.e. ground-penetrating radar (GPR)[6,7]. Urbini *et al.*[8] have used vehicle-mounted and heli-borne GPR in Antarctica to detect buried crevasses. Delaney *et al.*[9] and Nath *et al.*[10] have used this technology successfully for crevasse detection in Antarctica on a cold and dry snow pack. Eder *et al.*[11] have attempted crevasse detection using GPR in Alpine region. Taurisano *et al.*[12] have used GPR successfully between Norwegian Antarctic research station Troll and shelf ice region, to mitigate the crevasse hazard all along the route. According to Zamora *et al.*[13], the buried crevasses detected using GPR show apexes of diffraction hyperbolae and this can go up to 15 m depth. Luckman *et al.*[14] have successfully distinguished surface and basal crevasses using GPR and satellite imagery signatures.

Motivation for the study was to investigate techniques for crevasse detection in the Indian Himalayan glaciers (Figure 1) in order to delineate a safe route for mountain travellers. Radio echo sounding is a useful technique for detection of crevasses, as the conversion of snow into ice can be easily detected due to the change in density, water content and the dielectric constant. The feasibility and reliability of GPR for crevasse detection was investigated using a field study both in ground and airborne mode (Figure 2).

The GPR survey was carried out at Siachen (Karakoram Range) and Samudra Tapu (Great Himalayan Range) glaciers (Figure 1). The Siachen glacier in Karakoram Range with extensive development of crevasses is one of the largest glaciers in the Himalayan region. The length of the Siachen glacier is approximately 72 km and its width varies between 2 and 8 km. The glacier extends between altitudes 5400 and 3600 m. The seasonal snowfall in Siachen glacier area varies from 38 to 420 cm with a 22 years average of 197 cm. The mean seasonal air temperature varies from –14.3°C to –23.7°C with an average of –20°C (ref. 15).

The Samudra Tapu glacier (lat. 32°29.86′–32°26.9′N and long. 77°24.68′–77°36.43′E) lies in Chandra basin of the Great Himalayan Ranges. The approximate length of the glacier is 19 km and its width is 1 km. It has two flanks and both are of nearly equal length. The glacier extends between 4100 and 5400 m in elevation. It is largely moraine-free and ingested with a large number of crevasses. The mean seasonal temperature of this region varies between –5.9°C and –10.7°C with 22 years average of –8.7°C. Seasonal snowfall varies between 134 and 410 cm with 22 years average of 261.5 cm (ref. 15).

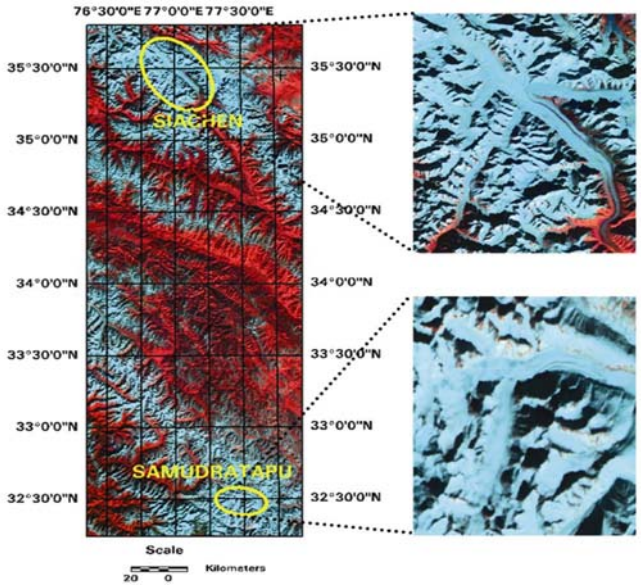

Figure 1. Location of glaciers surveyed for crevasse detection in the Indian Himalaya.

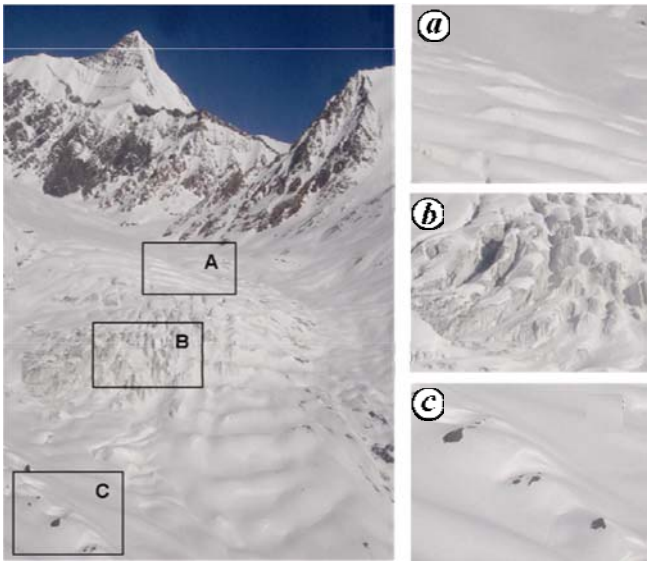

Figure 2. Field photograph showing various features of Samudra Tapu glacier. ***a***, Hidden crevasse; ***b***, Open crevasse; ***c***, Buried boulder.

In the present study, Ramac GPR from Mala Geoscience (www.malagas.com) and Radarteam antenna (www.radarteam.se) were used for ground and airborne surveys respectively. The Ramac GPR with 250 MHz center frequency antenna was used to obtain GPR profiles in ground mode from the Siachen glacier. The survey was conducted between 12 and 20 February 2003 in approximate 10 sq. km area near snout. The dimension of the 250 MHz antenna is 780 mm × 440 mm × 160 mm, with approximate weight of 8 kg. The antenna is a bow-tie type, shielded (monostatic) and having the transmitter and receiver at around 0.31 m distance. One wheel is attached at the rear of the antenna, which acts as a trigging device instructing the antenna to collect traces at preset intervals and is also used for length measurement. The data are collected by dragging the antenna over the surface. The time windows (159 and 198 ns) with sampling frequencies of 2395–2695 MHz and trace interval 0.018–0.040 m were the survey parameters used for collection of crevasse signatures. Data are stored in 16-bit integer raw data format and are further transferred from control unit to a laptop using standard parallel port. Each electronic component, except the laptop, is powered by rechargeable Ni–Cd and Pb batteries.

The 350 MHz centre frequency hemispherical butterfly dipole antenna (M/S Radarteam, Sweden) was used in airborne mode. The antenna was top-shielded and designed to take measurements from the airborne platform. The overall dimension of the antenna mounted at the base of the helicopter is 740 mm × 405 mm × 225 mm, with approximate weight of 6 kg. A GSSI data acquisition system, i.e. Subsurface Interface Radar 3000 (SIR 3000) was used for acquiring the survey data. To run the entire GPR system a 10.8 V lithium-ion rechargeable battery pack was used for the power supply. The helicopter height was maintained nearly at a constant level of 40 m from ground with an average speed of 18 m/s during the survey, so that the reflected signatures can be captured within the available fixed time window of SIR 3000 unit. For the 350 MHz GPR antenna, the optimum time-window size was fixed at 120 ns. In order to remove the air medium from radar profiles, an offset value was subtracted from the raw data. In air, the two-way-travel (TWT) time is 7 ns corresponding to an offset of 1 m air thickness. Therefore, the offset value against 40 m thick air medium (height of helicopter from ground) was kept constant at 280 ns during the survey. The survey parameters for GPR data acquisition were selected as 512 samples/scan with a scan rate of 64 scan/s. To synchronize the SIR 3000 unit with GPS system a triggering device (TRG-817) was used. The marker software (GeoPointer X) supported by Toughbook (TB), controls the trigger pulses through TRG-817 and it was connected via an USB cable to the TB. The spatial data were recorded in the TB via RS 232 interface according to the geographic positions measured by GPS.

Table 1. Electromagnetic wave properties in different media[20]

Medium	ε (rel)	σ (ms/m)	V (m/ns)	α (db/m)
Air	1	0	0.3	0
Freshwater	80	0.5	0.033	0.1
Seawater	80	30000	0.01	1000
Snow	2–3.5	0.00001	0.20	0.01–0.1
Ice	3–4	0.01	0.16	0.01
Clay	5–40	2–1000	0.06	0.01

ε = dielectric constant, σ = electrical conductivity, V = wave velocity and α = attenuation coefficient.

The velocity of the radar wave which is required for estimation of depth of the medium, varies with the dielectric permittivity of the medium. The velocity (v) at which the electromagnetic (EM) wave travels through medium is given by

$$v = c/(\varepsilon_r)^{1/2}, \quad (1)$$

where c is the speed of light (3×10^8 m/s).

EM wave velocity is greatest in vacuum and decreases with increasing dielectric constant. In order to analyse the results of radio-echo sounding, velocity of propagation of radio waves in ice is used (Table 1). A technique was proposed by Robin *et al.*[16] to relate different ice parameters (density, ice fabric and temperature) to the velocity of radio waves in ice. Estimated velocity reported was ~ 0.167 ± 0.3 m/ns at –20°C. The same range of velocity of radio waves in ice was also observed by Jiracek and Bentley[17]. In the present work the GPR profiles were processed assuming velocity of EM wave in ice as 0.168 m/ns. Velocity information is further used to calculate expected TWT of reflection using the relationship

$$\mathrm{TWT} = 2d/v, \quad (2)$$

where d is the distance to the reflector.

The used antenna frequencies of 250 and 350 MHz are well suited for crevasse detection because of their penetration depth, spatial resolution, vertical resolution and size of antennas. The penetration depth of EM wave in a medium is the inverse of extinction coefficient[18]. The extinction coefficient consists of an absorption coefficient and a scattering coefficient. In the microwave region for snow/ice, the scattering coefficient is negligible in comparison to the absorption coefficient.

The penetration depth (δ_p) can be estimated by the relation

$$\delta_p = 1/X_a, \quad (3)$$

where X_a is the absorption coefficient, which can be defined as

$$X_a = (2\pi/\lambda)(\varepsilon''/\sqrt{\varepsilon'}), \quad (4)$$

where λ is the wavelength of the EM wave in ice, ε'' is the imaginary and ε' the real part of the complex dielec-

tric constant of ice. The values of ε'' and ε' used in the study are 0.007 and 3.17 respectively. Using a 250 MHz frequency the depth of penetration within ice media is found to be ~27 m; however, for 350 MHz it becomes 19 m approximately. The vertical resolution for 250 and 350 MHz antennas is 0.34 m and 0.24 m respectively. Thus due to sufficient penetration power in ice medium, good vertical resolution and suitable size of antennas, the frequencies 250 and 350 MHz were selected for the study.

The locations of all collected GPR profiles from Samudra Tapu glacier are shown in Figure 3. The airborne GPR survey on Samudra Tapu glacier was conducted between 15 and 25 March 2010. The survey profiling was carried out along and across the glacier, and 50–55 profiles along and 20–30 profiles across the glacier were collected. A distance of approximately 10 m between different profiles was kept during the survey. However, due to limitation of the helicopter flying in such a rugged terrain, this distance sometimes varied between 5 and 20 m. In the radar profiles hyperbolic signatures were obtained, which may be from buried point objects, void and from any discontinuity in the glacier. These hyperbolic signatures in the GPR profiles are because of the fact that in the GPR data acquisition it is generally assumed that a reflected signal comes from directly beneath the antenna; however, radar antennas always operate with more or less conical beams. Thus, the GPR observes the target from different angles while traversing and record the returned signal assuming the object directly underneath the antenna. Thus GPR produces hyperbolic signature for buried object.

The methodology for crevasse detection is given in Figure 4. The observed hyperbolic signatures in GPR profiles collected in Siachen glacier were validated on ground. During the ground mode GPR survey we were able to collect the signatures of open and hidden crevasses but also observed some limitations of the equipment while using on glacier surface. To avoid one such problem of skidding antenna wheel on the glacier ice, the survey was conducted at very low speed. Hence, only a small area of the glacier could be surveyed. To collect crevasse signatures from larger area of a glacier, airborne GPR survey was conducted over Samudra Tapu glacier. The hyperbolic signatures (discontinuities) in airborne GPR profiles from Samudra Tapu glacier were validated with high-resolution optical satellite image (Cartosat-1) and Survey of India (SOI) map. The satellite images have been used for identification of surface features on ice media since the earliest satellite missions[19]. Radarsat-2 SAR data were used to discriminate between hidden crevasses and buried boulder signatures. On the basis of airborne GPR and SAR data, a criterion for crevasse detection was developed. Validation of the identified crevasse zones and buried boulder area was done using Cartosat-1 image and SOI map. After validation the crevasse map of the Samudra Tapu glacier was prepared.

The criteria for crevasse detection are as follows: (a) Hyperbola in radargram at the top corresponds to open crevasse. (b) Hyperbola in radargram at depth and backscattering value (SAR) less than – 12 db corresponds to hidden crevasse. (c) Hyperbola in radargram at depth and backscattering value (SAR) greater than – 12 db corresponds to boulder.

The GPR data collected in ground mode at Siachen glacier were processed using the Ground vision software and wave velocity of 0.168 m/ns in the medium was used. In post-processing, to amplify the dynamical range of the data display, a top mute of first arrivals corresponding to the direct wave was performed. To remove the dark current, which is the constant offset in the amplitude of the registered trace the DC filter was used and finally background filter was used to eliminate temporally consistent noise from the complete profile.

Post-processing of the airborne profiles was carried out using Reflex 2D Quick software. In order to enhance the weak signals, a gain function was used in both pre- and post-processing radar profiles. Filters such as subtract DC shift, bandpass butterworth (lower cut-off 100 MHz and upper cut-off 1000 MHz), fk migration (Stolt) and background removal were applied on the airborne GPR data during post-processing. The geographic positions were imported in a tabular format with the help of Reflex 2D Quick software and the data were superimposed on radar profiles (*.DZT format).

The SAR works independent of the solar illumination and unlike the optical sensor, provides the volume information of the targetted surface. Radarsat-2 (C-band) level-1 data of path image (SAR Georeferenced) in standard acquisition mode of 24 February 2011 was used in the present study. Table 2 provides a brief description of Radarsat-2 data used in the study. Data were processed using software provided by the European Space Agency

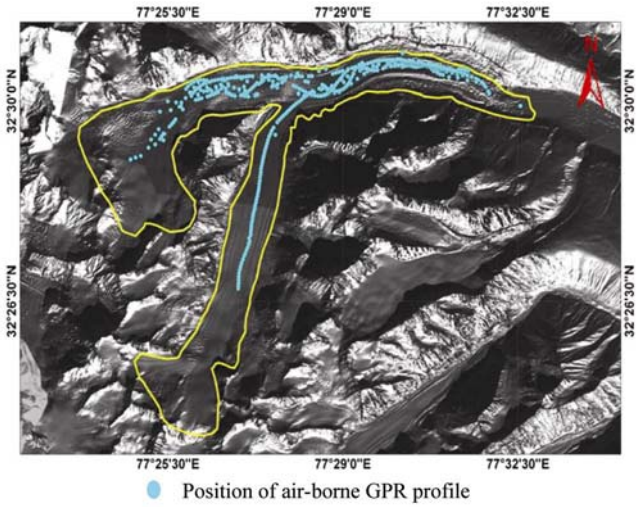

Figure 3. GPS points overlaid over Samudra Tapu glacier showing the positions corresponding to the airborne GPR profiles.

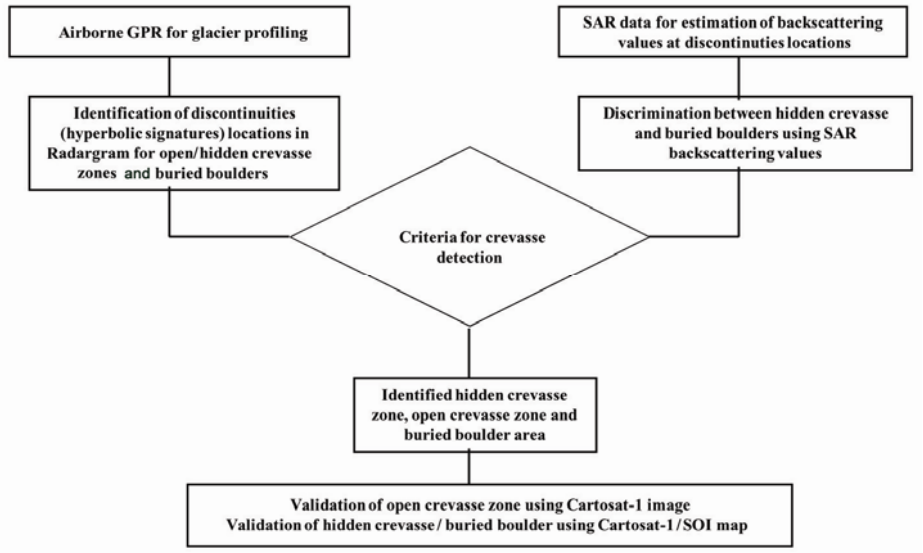

Figure 4. Flow chart of methodology for crevasse detection.

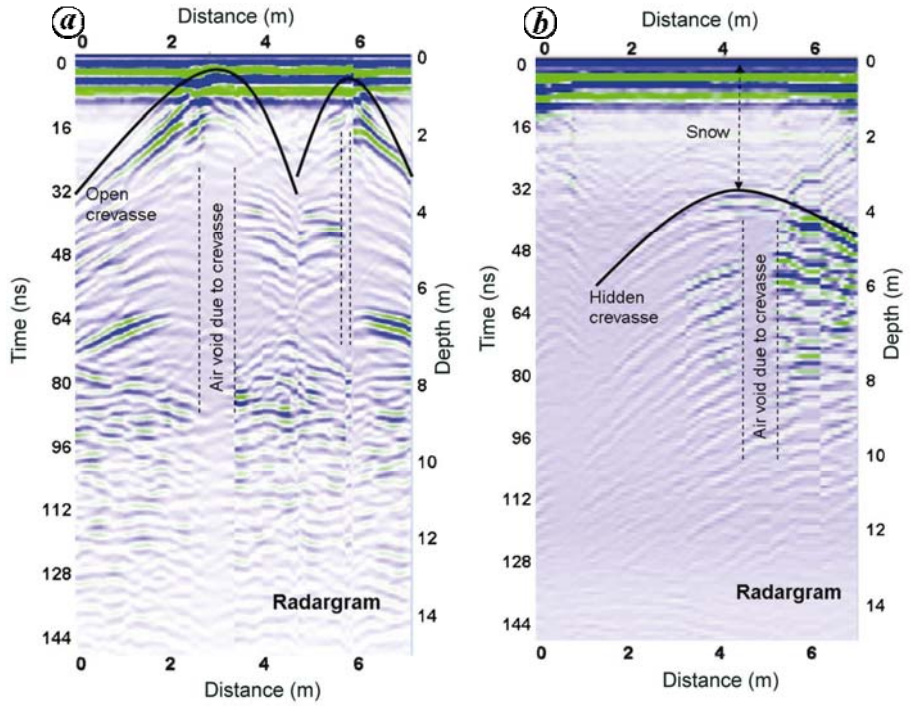

Figure 5. Radargram showing signature of open crevasse (***a***) and hidden crevasse (***b***) collected in ground mode from Siachen glacier.

Table 2. Specification of Radarsat-2 data product

Parameter	Value
Sensor and frequency	Radarsat-2 and 5.35 GHz
Nominal swath width (km)	100
Nominal spatial resolution (ground range × azimuth; m)	25 × 28
Pixel spacing (azimuth × range; m)	12.5 × 12.5
Incidence angle (near and far range)	30° and 37°
Polarization	HH, HV

(ESA; Next ESA SAR Toolbox-NEST v4B). The digital number (DN) values of intensity image are converted to corresponding radar backscattering coefficient (σ^0). The parameters which influence the radar backscatter, i.e. inherent speckled appearance, satellite ground-track, incidence angle, radar polarization and surface roughness are considered in the analysis.

Inherent speckle appearance was removed through multilooking process; the number of looks in azimuth and

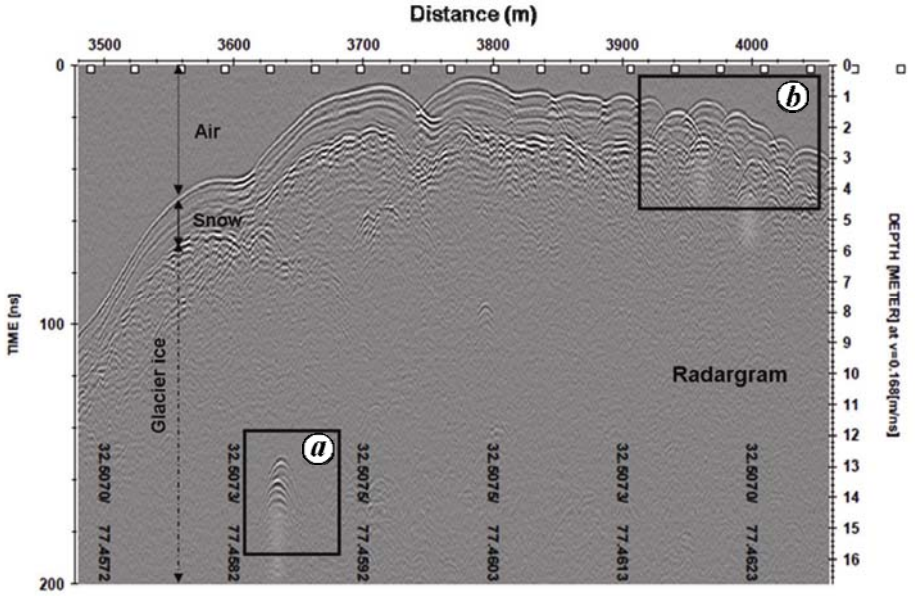

Figure 6. Radargram of airborne GPR profile collected from Samudra Tapu glacier ***a***, Hidden crevasse, ***b***, Open crevasse.

range of scene being 4 and 1 respectively. The radar scattering noise was removed by applying a mean 3×3 kernel filter. For the retrieval of σ^0 values geometric and radiometric terrain corrections were applied on data.

Geometric terrain correction was performed using Range Doppler Terrain Correction operator, which uses orbit state vector information in the metadata, the radar timing annotations, the slant to ground range conversion parameters together with the reference DEM data to derive the precise geolocation information. Radiometric normalization was implemented to get the corrected σ^0 values by considering scattering area, antenna gain pattern and range spread loss.

Ground-mode GPR experiments for crevasse detection are important as onsite validation of the collected GPR profiles can be done. Figure 5 shows the Radargram of GPR profiles collected in ground mode from crevasse-prone areas of Siachen glacier. The discontinuities in the form of hyperbolic signatures as observed in Figure 5 *a* are found overlapped with the first reflected wave, i.e. the reflected wave from the ice surface. These hyperbolic signatures (02 numbers) in the Radargram are due to the open crevasse as no snow accumulation is observed over the void. In the radargram the horizontal axis is the calibrated horizontal distance travelled across the crevassed area. The vertical axis on the left is TWT (in ns), whereas on the right a depth scale (in m) is indicated considering an airwave velocity in ice of 0.168 m/ns. The sets of diffraction hyperbola centred at approx. 3 and 6 m correspond to the prominent crevasses detected on the surface and the width of these crevasses is approximately 0.70 and 0.20 m respectively. In the radargram the air-filled cavity having no reflection can also be seen. The crevasse walls as observed in the radargram are smooth and show no visible distortion.

In Figure 5 *b*, a hyperbolic discontinuity in the radargram is observed at 3.8 m depth. This hyperbolic signature is due to the hidden crevasse which was covered by a snow bridge of 3.8 m. The apex of diffraction hyperbola is observed at around 4.2 m in the radargram. Feeble reflections due to rising snow layers were observed near the crevasse location and high-amplitude reflections were observed from the snow–ice interface. Further the air-filled void signatures were observed in the radargram as in the open crevasse. The crevasses dipping snow layer reflections and strong diffractions from depth were also observed. The width of the hidden crevasse was found to be approximately 0.75 m. In order to estimate the exact snow thickness deposited over the crevasse the wave velocity for dry snow, i.e. 0.237 m/ns (ref. 20) was used as the snow deposited on the glacier was dry. This wave velocity result indicates snow bridge thickness as 4.3 m. Thus the possible error in estimation of snow thickness over the crevasse is 11%. However, such thickness of the snow bridge, 3.8–4.3 m can be considered as safe to travel.

An unsmooth glacier surface (fractured ice zone) was visually observed at few points during collection of airborne GPR data, which may probably be due to the presence of open crevasses. Figure 6 shows the radargram of one of the airborne GPR profile data collected among the various longitudinal and transverse profiles as marked in Figure 3. In Figure 6 two interfaces are clearly visible, i.e. air–snow and snow–ice. The total penetration of the signal was observed ~ 16 m corresponding to the 200 ns time window for the 350 MHz antenna. Various hyperbolic signatures can be observed at the air–snow interface

and from deep inside the glacier ice. The hyperbolic signatures observed near the air–snow interface are marked with square B and these may correspond to the open crevasses present over the glacier surface. Diffraction hyperbolae associated with prominent open crevasses are clearly observed while traversing between 3910 and 4050 m in the radargram (Figure 6). Due to the large number of hyperbolas in this region, it is marked as the open crevasse zone. However, the hyperbolic signatures or the discontinuity originating from within the glacier ice as marked in square A in the radargram may be due to the hidden crevasse. This detected discontinuity in radargram is buried inside 1.5 m snow and 8 m of ice mass.

Radarsat-2 SAR satellite data of dated 24 February 2011 were used to discriminate between the hidden crevasses and boulders. Figure 7 shows the backscattering values corresponding to the observed discontinuity locations in the radargram. After analysing the backscattering values it was observed that the threshold value of backscattering that can differentiate between boulder and hidden crevasse is approximately –12 db. On the basis of the backscattering values from SAR data and air-borne profiles, the probable zones of buried boulders and hidden crevasses were identified over the glacier.

A crevasse map of the Samudra Tapu glacier has been prepared after analysing airborne GPR profiles and SAR data. The signatures corresponding to hidden crevasses, open crevasses and buried boulders according to their geographic locations were marked on the map (Figure 8). Both hidden and open-type crevasses were identified in the accumulation and ablation zones. In addition, close to the snout of the glacier various hyperbolic signaures were observed corresponding to certain unknown objects. In field validation at few places near the glacier snout, it was found that these unknown objects were big boulders. The same has been further verified by the high-resolution Cartosat-1 imagery and SOI mapsheet surveyed in 1979.

In order to validate the open crevasse zones as identified from the airborne GPR profiles, Cartosat-1 imagery having spatial resolution of 2.5 m dated 28 September 2009 was used. Figure 9 shows the image of various media observed on the Samudra Tapu glacier. As the open crevasses are linear feature on the glacier surface thus can be clearly identified in Cartosat-1 imagery by considering the shape, size and pattern as shown in Figure 9 *a*. In satellite image the hidden crevasses (Figure 9 *b*) were marked by identifying the depression zones in the snow that is covering the glacier ice, because in the glacier generally depression zones are created during the conversion of open crevasse into the hidden crevasse. In the satellite image rough and irregular surfaces were also observed and these surfaces according to their texture and contrast to glacier ice/snow were marked as boulders (Figure 9 *c*).

This hybrid technique consisting of radar in ground and air, high-resolution satellite imageries along with SOI maps and active microwave satellite data was found to be useful and successful for detection of crevasse-prone areas in a Himalayan glacier. The data collected and analysed from the ground-based survey at Siachen glacier for crevasse detection, were further used in the interpretation of airborne GPR results. The crevasse zones and other features identified using the combination of airborne GPR profiles and SAR data, were validated using Cartosat-1 images and SOI maps, and they were found to be in good agreement. The thickness of the snow bridge over the glacier ice is the critical parameter for safety of persons moving on the glaciers, and this thickness is measured by GPR within an accuracy of 11%. The width of the crevasses identified in ground mode looks more realistic in comparison to airborne results. As the spatial resolution of 350 MHz antenna from 40 m height is > 3 m; it is difficult to identify the crevasses individually when they are closely spaced, say less than 3 m. There are chances that hyperbolic signatures due to various crevasses present in

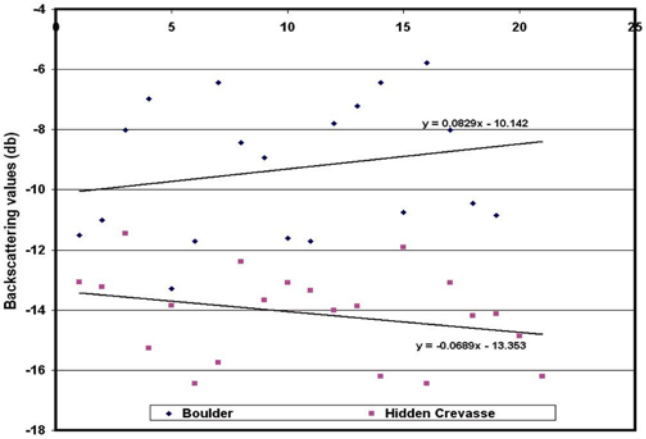

Figure 7. Backscattering values estimated using Radarsat-2 data to discriminate between hidden crevasse and buried boulders.

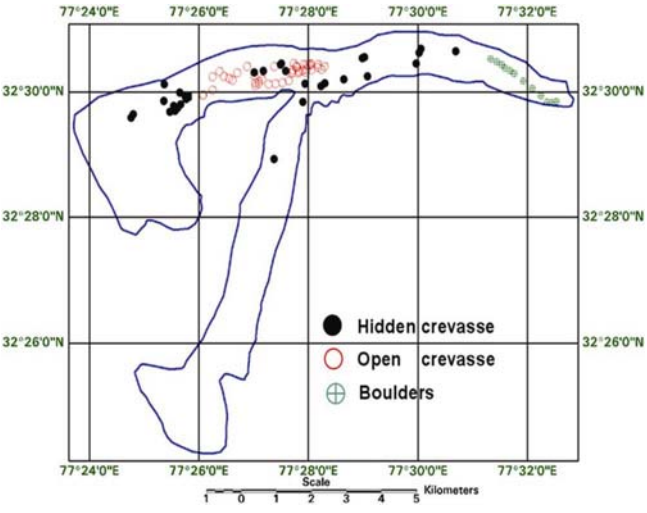

Figure 8. Identified crevasse zones and buried boulder areas in Samudra Tapu glacier.

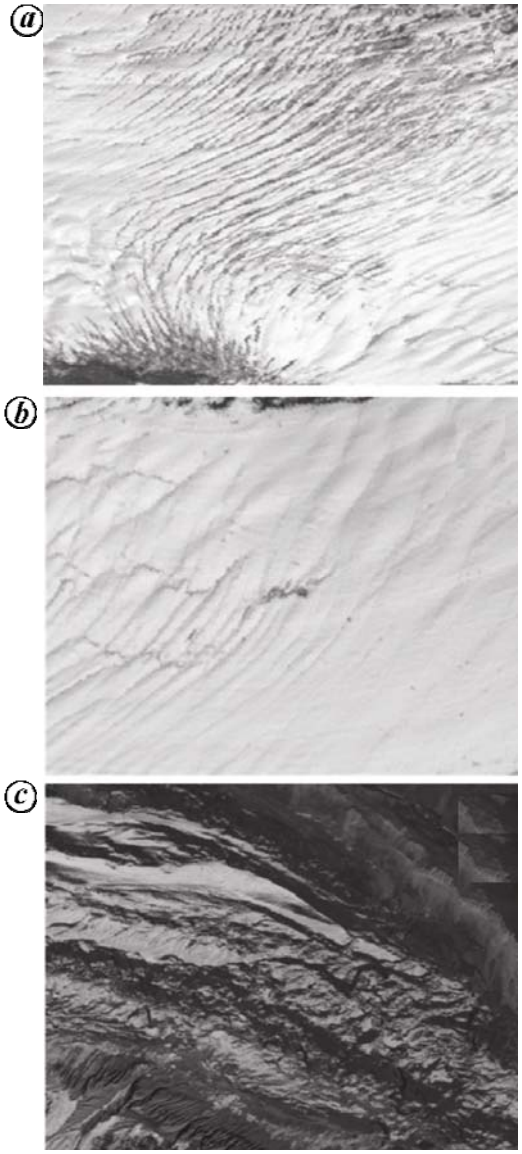

Figure 9. Identified glacier features in Cartosat-1 imagery. ***a***, Open crevasse; ***b***, Hidden crevasse; ***c***, Buried boulders.

a small area may have combined and produced bigger hyperbola. The bigger hyperbola in the radargram may correspond to a number of crevasses in spite of single crevasse, which may introduce error in estimation of crevasse size. Overall this multi-sensor based methodology can provide useful information of crevasse zone in glaciers, which is difficult to obtain using a single sensor or conducting a field survey. In the near future high-resolution DEM using lidar and areal photogrammetry in conjunction with high-resolution SAR data will be helpful to generate more detailed crevasse maps.

1. Paterson, W. S. B., *The Physics of Glaciers*, Elsevier Science, New York, 1994, pp. 187–190.
2. Holdsworth, G., Primary transverse crevasses. *J. Glaciol*., 1969, **8**, 107–129.
3. Hambrey, M. J. and Muller, F., Structures ice deformation in the White Glacier, Axel Heiberg Island, Northwest Territories, Canada. *J. Glaciol*., 1978, **29**, 41–66.
4. Vornberger, P. L. and Whillans, I. M., Crevasse deformation and examples from Ice Stream B, Antarctica. *J. Glaciol*., 1990, **36**, 3–9.
5. Harper, J. T., Humphrey, N. F. and Pfeffer, W. T., Crevasse patterns and the strain-rate tensor: a high resolution comparison. *J. Glaciol*., 1998, **44**, 68–77.
6. Shabtaie, S. and Bentley, C. R., West Antarctic ice streams draining into the Ross Ice Shelf configuration and mass balance. *J. Geophys. Res*., 1987, **92**, 1311–1336.
7. Retzlaff, R. and Bentley, C. R., Timing of stagnation of Ice Stream C, West Antarctica, from short pulse radar studies of buried surface crevasses. *J. Glaciol*., 1993, **39**, 495–506.
8. Urbini, S., Vittuari, L. and Gandolfi, S., GPR and GPS data integration: examples of application in Antarctica. *Ann. Geofis.*, 2001, **44**, 687–702.
9. Delaney, A., Acrone, S., Bannon, A. and Wright, J., Crevasse detection with GPR across the Ross Ice Shelf, Antarctica. In Tenth International Conference of Ground Penetrating Radar, Delft, The Netherlands, 2004.
10. Nath, P. C. and Vaughan, D. G., Subsurface crevasse formation in glaciers and ice sheets. *J. Geophys. Res*., 2003, **108**, doi: 10.1029/2001JB000453.
11. Eder, K., Reidler, C., Mayer, C. and Leopold, M., Crevasse detection in alpine areas using ground penetrating radar as a component for a mountain guide system. *Int. Arch. Photogramm., Remote Sensing Spatial Inf. Sci*., 2008, **37**, 837–842.
12. Taurisano, A., Tronstad, S., Brandt, O. and Kohler, J., On the use of ground penetrating radar for detecting and reducing crevasse-hazard in Dronning Maud Land, Antarctica. *Cold Reg. Sci. Technol*., 2006, **45**, 166–177.
13. Zamora, R. *et al.*, Crevasse detection in glaciers of southern Chile and Antarctica by means of ground penetrating radar. In *Glacier Mass Balance Change and Meltwater Discharge*. IAHS assembly in Foz do lguacu, Brazil, 2005, IAHS Publ. 318, 2007.
14. Luckman, A., Jansen, D., Kulessa, B., King, E. C., Sammonds, P. and Benn, D. I., Basal crevasse in Larsen C ice shelf and implications for their global aboundance. *The Cryosphere*, 2012, **6**, 113–123.
15. Gusain, H. S., Chand, D., Thakur, N. K., Singh, A. and Ganju, A., Snow avalanche climatology of Indian Western Himalaya. In Proceedings of the International Symposium on Snow Monitoring and Avalanches, SASE Manali, 6–10 April 2009.
16. Robin, G. de Q., Velocity of radio waves in ice by means of borehole interferometric techniques. *J. Glaciol*., 1975, **15**, 151–160.
17. Jiracek, G. R. and Bentley, C. R., Velocity of electromagnetic waves in Antarctic ice. *Antarct. Res. Ser*., 1971, **16**, 199–208.
18. Stiles, W. H. and Ulaby, F. T., Dielectric properties of snow. The University of Kansas, Center for Research, Inc., Remote Sensing Laboratory, Technical Report 527-1, 1981.
19. Crabtree, R. D. and Doake, C. S. M., Flow lines on Antarctic ice shelves. *Polar Rec*., 1980, **20**, 31–37; doi: 10.1017/S00322474 00002898.
20. Davis, J. L. and Annan, A. P., Ground-penetrating radar for high resolution mapping of soil and rock stratigraphy. *Geophys. Prospect*., 1989, **37**, 531–551.

ACKNOWLEDGEMENTS. We thank R. K. Garg, Jimmy Kansal, M. R. Bhutiyani, P. Datt, Hari Ram and S. K. Dewali for technical support; Ramanand Singh, Karamjeet, Anek Singh and Aswani for GPR data collection, and the helicopter pilots and crew members for their support in flying over highly rugged mountainous terrain according to our survey requirements.

Received 14 December 2012; revised accepted 30 August 2013